Petroleum Science 20 (2023) 3865–3874

Contents lists available at ScienceDirect

Petroleum Science

journal homepage: www.keaipublishing.com/en/journals/petroleum-science

Original Paper

Encapsulation of ionic liquid, phosphotungstic acid inside the nanocages of MIL-101(Cr): Effective and reusable catalyst for efficient solvent-free oxidative desulfurization from fuel oil

Bo-Long Jiang [a, *], Dong-Xu Zhang [b], Dan-Dan Yuan [b], Yan-Guang Chen [b], Tian-Zhen Hao [c], Hua Song [b, **]

[a] Innovation Institute for Sustainable Maritime Architecture Research and Technology, Qingdao University of Technology, Qingdao 266000, Shandong, China
[b] Provincial Key Laboratory of Oil & Gas Chemical Technology, College of Chemistry & Chemical Engineering, Northeast Petroleum University, Daqing 163318, Heilongjing, China
[c] Hebei Jingzhi Technology Co., LTD, Cangzhou 061000, Hebei, China

ARTICLE INFO

Article history:
Received 22 March 2022
Received in revised form
9 April 2022
Accepted 26 July 2023
Available online 27 July 2023

Edited by Jia-Jia Fei and Teng Zhu

Keywords:
Metal organic frameworks
Phosphotungstic acid
Ionic liquids
Stability
Oxidative desulfurization

ABSTRACT

Oxidative desulfurization from fuel oil is one of the important methods for deep desulfurization. The development of efficient oxidative desulfurization catalysts is crucial for improving the desulfurization performance. Successful encapsulation of phosphotungstic acid (HPW) and ionic liquid (BMImBr) inside the mesoporous cages of MIL-101(Cr) was accomplished through a combination of "bottle around ship" and "ship in bottle" methods. The obtained BMImPW@MIL-101(Cr) composite was characterized by XRD, FTIR, BET, SEM, XPS and ICP methods. Results indicated that the BMImPW@MIL-101(Cr) composites with PW^{3-} loading of 23.1–50.7 wt% were obtained, demonstrating that the "bottle around ship" method is beneficial to make full use of nanocages of MIL-101(Cr) to obtain expected high loading of active PW^{3-}. The BMImPW@MIL-101(Cr) exhibits excellent reusability with no evidence of leaching of active PW^{3-} and $BMIm^{+}$, and well-preserved structure after successive cycles of regeneration and reuse. The significantly improved stability of BMImPW@MIL-101(Cr) as compared to HPW@MIL-101(Cr) is possibly because the leaching of the active PW^{3--} sites can be greatly suppressed by forming large size of BMImPW owing to introduction of $BMIm^{+}$ cation. The BMImPW@MIL-101(Cr) exhibited excellent catalytic activity for solvent free oxidative desulfurization of refractory sulfides. The enhanced oxidative desulfurization activity as compared to HPW@MIL-101(Cr) can be explained by the intimate contact of sulfides with active PW^{3-} sites owing the strong attraction of $BMIm^{+}$ cation with the sulfides.

1. Introduction

Petroleum is one of the most important industrial raw materials, which were used in many aspects of daily lives (Qi et al., 2023; Zhu et al., 2023). The combustion of low-quality fuel oil obtained from petroleum leads to the emission of SO_x gases, causing a serious environmental problem. For these reasons, governments worldwide formulate increasingly stringent conditions on the sulfur content for fuel oils (Rajendran et al., 2020). Consequently, deep desulfurization of fuel oil has turned to be an environmentally urgent problems worldwide (Zhang et al., 2020). Comparing with other desulfurization methods, oxidative desulfurization (ODS) has received a great deal attention owing to its desirable characteristics of mild operating conditions and desirable removal efficiency for thiophenic compounds.

Up to now, a variety of catalysts has been developed for ODS, including metal oxides (Liu et al., 2019; Zhang et al., 2019a), titanosilicate (Shi et al., 2019), simple acids (Timko et al., 2016), polyoxometalates (POMs) and Heteropoly acids (HPAs) (Zhu et al., 2014, 2015; Li et al., 2019a), and solid composites (Ribeiro et al., 2019; Li et al., 2020). Among them, the HPAs, especially phosphotungstic acid ($H_3PW_{12}O_{40}$, HPW) with tunable acid-base and redox properties, and environmental compatibility have been widely

* Corresponding author.
** Corresponding author.
E-mail addresses: jiangbolong@qut.edu.cn (B.-L. Jiang), songhua2004@sina.com (H. Song).

https://doi.org/10.1016/j.petsci.2023.07.018

concened (Te et al., 2001; Mirante et al., 2018). However, the HPW presents several defects, such as the low surface area (1–10 m^2/g), tendency to agglomerate and difficulty of separating it from the reaction system, which restrict its wide application. There are many reports on heterogenization of HPW onto porous materials (zeolites, metallic oxides and carbons) (Li et al., 2016; Yue et al., 2018; Rajendran et al., 2020; Wang et al., 2020; Shan et al., 2021). Although heterogenization of HPW onto these supports makes the catalyst easy to recycle, the leaching of HPW cannot be prevented, which lead to a poor stability. The leaching can be solved by encapsulating HPW into zeolitic cavities since the HPW clusters are larger than the open windows of the zeolitic nanocages. Unfortunately, only very low HPW loading can be reached (<5 wt%), which leads to a poor activity (Zhang et al., 2015).

Metal-organic frameworks (MOFs) have been regarded as a fascinating porous materials and can be used in many field (Gu et al., 2012; Li et al., 2019b). The intrinsic activity of coordinatively unsaturated sites can also be served as anchoring points for molecules (Juan-Alcaniz et al., 2012). Besides, the high surface area and regular structure favor the periodically dispersion of the active sites, while the tunable cages make them the promising candidate for host matrices to encapsulate HPW with high content (Wang et al., 2014). The encapsulation of HPW into the cages of the MOF has been studied (Liu et al., 2013; Ding and Wang, 2016; Li et al., 2018). For instance, Hu et al. (2013) prepared HPW(3.5)@MIL-101(Cr) with HPW loading of 17 ~ 50 wt% via a "bottle around ship" (also known as "one-pot procedure") method. Although HPW was encapsulated inside the cavities of MIL-101(Cr), the leaching of active HPW, though not severe, was still observed (approximately 9 wt% after four consecutive ODS cycles). Therefore, it is necessary and worthwhile to further study the method of firmly encapsulating HPW inside MOFs cages.

An effective way to solve this problem is to replace HPW cation with larger size cations. Ionic liquids (ILs) were used for ODS in recent years since they are environmentally friendly solvents (Huang et al., 2010; Wang et al., 2010a). Some researchers synthesized a PW-based catalyst in which a lipophilic IL was introduced by ionic exchange and found that the introduction of the IL can improve the stability of PW^{3-} and prevented the necessity of using other organic solvents (Zhu et al., 2011; Yuan et al., 2017). There are three approaches for preparing IL-based or HPA-based porous materials: impregnation, "ship in bottle" and "bottle around ship", respectively (Juan-Alcaniz et al., 2012). Wan et al. (2015) synthesized $[SO_3H\text{-}(CH_2)_3\text{-}HIM]_3PW_{12}O_{40}$@MIL-100(Fe)] catalyst by "bottle around ship" method. The as prepared catalyst presented a relatively high esterification activity of oleic acid and good regeneration ability due to the absence of any noticeable leaching of the active component. Khan et al. (2017) synthesized IL@ MIL-100(Fe) by assembling the ILs inside of the pores of MOF, namely the "ship in bottle" approach. HPA was then encapsulated into the IL@MIL-100(Fe). They found that the obtained IL/HPA@MIL-100(Fe) composites were stable during the adsorption/regeneration cycles. However, the loading of HPA was only ~20 wt%, which is low for ODS catalyst. It's worth noting that the dimensions of Keggin POMs (13–14 Å diameters) are smaller than the hexagonal windows (16 Å pore sizes) of large mesoporous MIL-101cages, and larger than pentagonal windows (with a free opening of 12 Å) of small MIL-101cages (Maksimchuk et al., 2012). Therefore, with the post introducing HPA into the MIL-101 approach, HPA guest could only enter into the large cages, which lead to a low loading of HPA. In addition, the leaching of HPA during ODS could not be prevented because the size of HPA is smaller than the cage windows.

Our group (Zhang et al., 2019b) prepared HPW/MIL-100(Fe) catalysts (HPW loading of 30~50 wt%) by "bottle around ship" method for ODS process from fuel oil such as gasoline and diesel. Results showed that the catalyst with HPW loading of 40% showed the best ODS activity, but the ODS activity retained only 63% after fourth cycle. Based on the studies that are mentioned above, a new method for synthesizing highly active and stable composites from the 1-*n*-butyl-3-methylimidazole bromide IL (BMImBr), HPW and MIL-101(Cr) for ODS with H_2O_2 as oxidant was proposed. HPW is encapsulated inside the cages of the MIL-101(Cr) by "bottle around ship" HF-free method, which can make HPW guest enter into both of the small and large cages of MIL-101(Cr). As a result, the high loading and better dispersion of active HPW can be achieved, which thus provides more active HPW for ODS. The BMImBr was then introduced by the "ship in bottle" method to synthesize BmimPW@MIL-101(Cr), in which HPW act as a bridge to react with the BMImBr, which diffuse into the cages of MIL-100, by ion exchange. The formed BmimPW clusters are large enough to be firmly confined inside the mesoporous cavities, as a result, the leaching of HPW can be greatly alleviated. Furthermore, the BmimPW@MIL-101(Cr) are amphiphilic composite with the $Bmim^+$ act as hydrophobic group and the $PW_{12}O_{40}^{3-}$ act as hydrophilic group, which could greatly improve the interactions between organic sulfur molecular and catalyst. This would lead to enhanced reaction kinetics. As expected, the obtained BmimPW@MIL-101(Cr) catalyst showed outstanding ODS activity and reusability owing to the synergistic effect of $BMIm^+$, HPW and MIL-101(Cr).

2. Experimental section

2.1. Materials

Ethanol absolute and N, N-dimethylformamide (DMF) were purchased from Liaoning Quan Rui Reagent Co., Ltd. 1-Methylimidazole (99%), *n*-alkyl Bromide (CP, >98%), Chromic Nitrate ($Cr(NO_3)_3\cdot 9H_2O$, 99%) and phosphotungstic acid (HPW, AR) were obtained from MΛCKLIN. P-Phthalic acid (H_2BDC, 99%) and 1-*n*-butyl-3-methylimidazole bromide (BMImBr) were purchased from Aladdin. Hydrogen peroxide (H_2O_2, 30%) and *n*-Octane (AR) were supplied by Tianjin Damao Chemical reagent factory. Benzothiophene (BT, 98%), thiophene (TP, 99%), benzothiophene (BT), dibenzothiophene (DBT) and 4,6-dimethyldibenzothiophene (4,6-DMDBT) were provided by Energy Chemical Ltd., China.

2.2. Synthesis of catalysts

2.2.1. Synthesis of ionic liquids

Imidazole-based ionic liquid of BMImBr was synthesized by following a procedure. 1 mol of 1-bromobutane was gradually added to a flask with 1 mol of 1-methylimidazole and 100 mL DMF. The mixture was stirred at room temperature in a water bath for 6 h. After the reaction, the viscous liquid was purified by vacuum rotary evaporation at 70 °C. The clear crystal was obtained by washing with a large number of ether.

2.2.2. Synthesis of HPW(x)@MIL-101(Cr)

The HPW(3.5)@MIL-101(Cr) was synthesized through "bottle around ship" HF-free method (Fig. 1). 4.8 g of $Cr(NO_3)_3\cdot 9H_2O$, 2.0 g of H_2BDC and HPW (x = 2.0, 3.5 and 5.0 g) were dissolved in an 100 mL teflon-lined autoclave containing 60 mL distill water, and then was reacted at 220 °C for 12 h. After cool to room temperature, the resulting green precipitate was filtrated, washed and dried overnight at 150 °C to obtain the HPW(x)@MIL-101(Cr), where x (g) is the amount of HPW.

2.2.3. Synthesis of BMImPW(x)@MIL-101(Cr)

As shown in Fig. 1, the BMImPW(x)@MIL-101(Cr) composite was

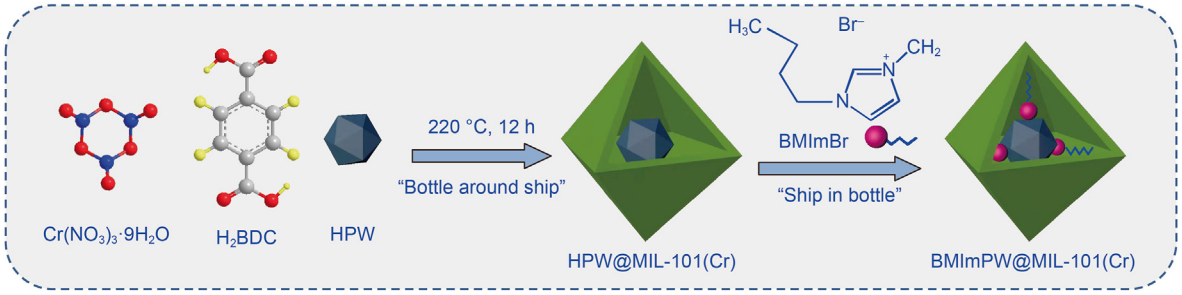

Fig. 1. Synthesis of BMImPW@MIL-101(Cr)

synthesized from HPW(x)@MIL-101(Cr) and ionic liquid (BMImBr). In a typical experiment, the excess ionic liquid (BMImBr) was dissolved in 20 mL distill water, and treated under ultrasonic waves for 10 min to obtain solution A. Then 1 g of HPW(x)@MIL-101(Cr) was dispersed into the solution under mild stirring at room temperature for 9 h. The light green solid was collected, washed, and dried overnight at 60 °C to obtain BMImPW(x)@MIL-101(Cr) composite.

2.3. Characterization

X-ray diffraction (XRD) patterns were recorded on a D/max-2200PC-X-ray diffractometer using Cu Kα radiation scan range from 1° to 10° at a rate of 1°/min. Scanning electron microscopy (SEM) was carried out on a ZEISS, ΣIGMA HD/VP scanning electron microscopy. Fourier transform infrared (FTIR) data were recorded on a Tensor 27 spectrosmeter in the wavenumber range of 400–4000 cm^{-1}. The typical physicochemical properties of catalysts were obtained by Brunauer-Emmett-Teller (BET) method using micromeritics adsorption equipment of TRISTAR II 3020. The sulfur-containing compounds present in model oils were measured by Clarus 680 GC-FPD (Perkin Elmer). The XPS spectra were acquired using ESCALAB MKII spectrometer. The tungsten contents of catalysts were determined by inductively coupled plasma-optical emission spectrometry (ICP–OES) using a PerkinElmer Optima 2000DV instrument.

2.4. Oxidative desulfurization

The model oil with sulfur content of 500 mg/L was made by dissolving a certain amount of BT, DBT, 4,6-DMDBT or TP) in n-octane, respectively. Oxidative desulfurization (ODS) was carried out in a 50 mL flask containing 20 mL BT model oils. Typically, a certain amount of catalyst (0.24 g) and model oil (20 mL) were put into a 50 mL flask at a constant temperature (50 °C) under stirring, and 30% H_2O_2 (O/S molar ratio of 8) was then added. After reacting for a certain time, the resulting suspension was separated, and the sulfur concentration of supernatant liquor was detected using a gas chromatograph (Clarus 680 GC-FPD with a flame photometric detector, Perkin Elmer).

2.5. Catalytic regeneration

The spent catalyst was obtained through centrifugation and then purified by washing with distilled water. Finally, the catalyst was dried overnight at 60 °C for the next ODS reaction. The spent and regenerated catalysts were named as BMImPW(x)@MIL-101(Cr)-Sy and BMImPW(x)@MIL-101(Cr)-R, where S refer to spent catalyst, R refer to regenerated catalyst, and y refer to the cycle times.

3. Results and discussion

3.1. Catalysts characterization

3.1.1. XRD

Fig. 2 presents low angle X-ray diffraction (XRD) patterns of HPW, MIL-101(Cr), HPW(3.5)@MIL-101(Cr), and BMImPW(3.5)@MIL-101(Cr). For the HPW, the peaks observed at 6.5° and 8.5° could be attributed to HPW. The peaks of HPW were hardly observed in the HPW(3.5)@MIL-101(Cr) or BMImPW(3.5)@MIL-101(Cr) catalysts, suggesting that it was highly dispersed. The pristine MIL-101(Cr) showed the diffraction peaks at 2θ = 2.78°, 3.25°, 3.43° and 3.94°, which can be assigned to the (022), (113), (222) and (004) planes of MIL-101(Cr) phase (Lee et al., 2018; Rajati et al., 2018; Zhang et al., 2019b). The peaks at 2θ = 3.0°–5.0° evidenced the mesoporous characteristic of these samples. The HPW(3.5)@MIL-101(Cr) showed peaks at 2θ = 2.80°, 3.30°, 3.45° and 4.00°, which confirmed the structure of MIL-101(Cr) was well preserved. However, compared to those of the MIL-101(Cr), these peaks slightly shifted as owing to the introduction of PW^{3-} into the MIL-101(Cr) cavity (Wan et al., 2015). Similarly, the XRD spectra for BMImPW(3.5)@MIL-101(Cr) showed a further small red shift in those peaks after loading of $BMIm^{+}$. The adjacent lattice for the different crystallographic planes increased by introducing PW^{3-} and $BMIm^{+}$ into the MIL-101, showing encapsulation PW^{3-} and $BMIm^{+}$ into the nanocages of MIL-101 (Table 1).

3.1.2. FTIR

As can be seen in Fig. 3, for HPW, the typical Keggin

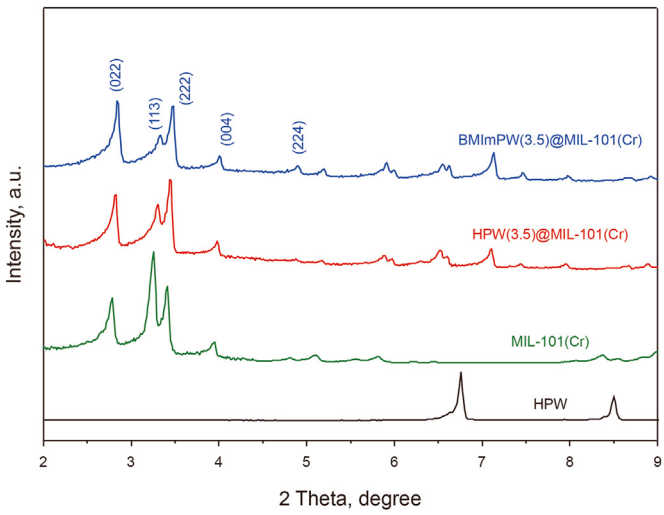

Fig. 2. Low angle XRD patterns of samples.

Table 1
The d-spacing according to the different crystallographic planes of catalysts.

Catalysts	d-spacing, nm				
	(022)	(113)	(222)	(004)	(224)
MIL-101(Cr)	3.1366	2.6759	2.5619	2.2190	1.8129
HPW(3.5)@MIL-101(Cr)	3.1733	2.7011	2.5847	2.2355	1.8678
BMImPW(3.5)@MIL-101(Cr)	3.1871	2.7087	2.5901	2.2394	1.8821

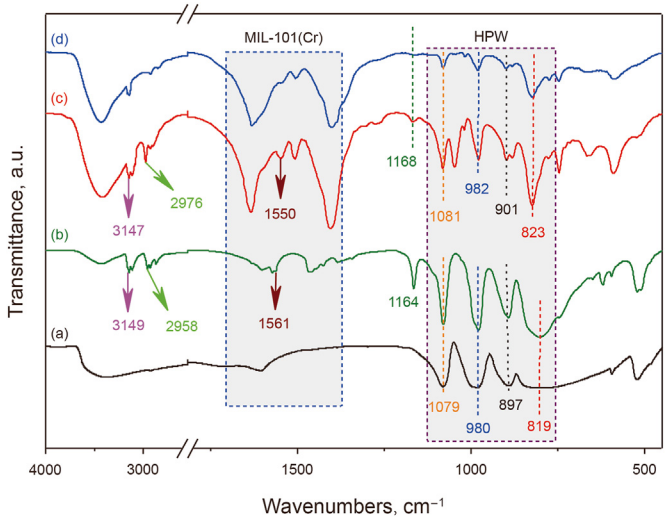

Fig. 3. FTIR spectra of (**a**) HPW, (**b**) BMImPW, (**c**) BMImPW(3.5)@MIL-101(Cr) and (**d**) HPW(3.5)@MIL-101(Cr)

characteristic peaks at 1079, 980, 897, and 819 cm^{-1} were observed, which could be assigned to P–O_a, W–O_d, W–O_b–W, and W–O_c–W stretching vibrations, respectively (Cardoso et al., 2004). For BMImPW, additional bands at 1164, 1561, 2958, and 3149 cm^{-1} appeared, which could be assigned to imidazole ring stretching, C=N stretching, C–H stretching on the substituent group, and C–H stretching on the imidazole ring, respectively. For HPW(3.5)@MIL-101(Cr), a set of bands in the range of 1200–1800 cm^{-1} are typical infrared peaks of MIL-101(Cr) (Xu et al., 2018), and the locations of Keggin characteristic peaks (1081, 982, 901, and 823 cm^{-1}) were slightly shifted as compared to those observed for HPW, confirming the successful encapsulation of HPW in the nanocages of MIL-101(Cr) (Liang et al., 2015). Furthermore, the FTIR spectrum of BMImPW(3.5)@MIL-101(Cr) presented bands of $BMIm^+$ (1168, 1550, 2976, and 3147 cm^{-1}), which were slightly shifted in band location compared to those for BMImPW, confirming the encapsulation of $BMIm^+$ in the nanocages of MIL-101(Cr) (Liang et al., 2015). As for the BMImPW(3.5)@MIL-101(Cr), the Keggin and $BMIm^+$ characteristic bands were both slightly shifted compared to the bands observed for BMImPW, showing the HPW and $BMIm^+$ were both successfully encapsulated in MIL-101(Cr).

3.1.3. BET

The N_2 adsorption-desorption isotherms of the three samples were well-defined with hysteresis loops, and could be classified type-IV isotherms (Fig. 4). In addition, the pore size distribution of MIL-101(Cr), HPW(3.5)@MIL-101(Cr), and BMImPW(3.5)@MIL-101(Cr) revealed main pore size at 2.51, 2.19 and 2.22 nm, respectively, which was decreased in the order MIL-101(Cr) > HPW(3.5)@MIL-101(Cr) > BMImPW(3.5)@MIL-101(Cr). These results proved that these samples had a uniform mesoporous structure.

The structural parameters of MIL-101(Cr), HPW(3.5)@MIL-101(Cr) and BMImPW(3.5)@MIL-101(Cr) are shown in Table 2. The surface area and pore volume of the parent MIL-101(Cr) were 2465 m^2/g and 0.93 cm^3/g, respectively, whereas for HPW(3.5)@MIL-101(Cr) the corresponding quantities were 1054 m^2/g and 0.31 cm^3/g, respectively. The significant decrease in surface area and pore volume further proved the encapsulation of HPW into the MIL-101(Cr) nanocages. Furthermore, compared to HPW(3.5)@MIL-101(Cr), the surface area and pore volume of BMImPW(3.5)@MIL-101(Cr) were further decreased owing to the encapsulation of $BMIm^+$ inside HPW(3.5)@MIL-101(Cr).

3.1.4. SEM

As shown in Fig. 5(a), MIL-101(Cr) showed a uniform octahedral geometry, which is in agreement with the previously reported morphology (Rajati et al., 2018), showing the MIL-101(Cr) structure was successfully obtained. For HPW(3.5)@MIL-101(Cr) (Fig. 5(b)) and BMImPW(3.5)@MIL-101(Cr) (Fig. 5(c)), the octahedral structure of MIL-101(Cr) was basically preserved, which indicates that the prestine crystal structure of MIL-101(Cr) was not destroyed after encapsulating HPW and BMIm.

3.2. ODS performance of catalysts

3.2.1. Comparison of different catalysts

The ODS performances of different catalysts were compared using 0.012 g/mL of catalyst in model oil and O/S molar ratio of 8 at 50 °C. It can be seen from Fig. 6 that a very low BT removal of 7.9% was obtained for MIL-101(Cr) within 150 min. For HPW, the BT removal was only 30.1% within 150 min owing to the poor dispersion. While for HPW(3.5)@MIL-101(Cr) and BMImPW(3.5)@MIL-101(Cr) catalysts, the BT removals were 68.0% and 72.1% within 60 min, respectively, showing the introduction of IL could accelerated the ODS speed. After an additional 150 min, both catalysts achieved 100% BT removal, which is much higher than that of HPW catalyst (32.5%). The high ODS performance of HPW(3.5)@MIL-101(Cr) is possibly because of the improved HPW active sites dispersion owing to high surface area, regular and tunable pore structure of MIL-101(Cr). Furthermore, the diffusion of reactants and products promoted by the tunable pores of MIL-101(Cr), which are beneficial for ODS (Khan et al., 2017). As for the improved ODS activity of BMImPW(3.5)@MIL-101(Cr) owing to the introduction of IL will be discussed later in section 3.4.

3.2.2. Effect of PW^{3-} loadings and ODS conditions

Effect of PW^{3-} loadings on the BT ODS performance over BMImPW(*x*)@MIL-101(Cr) is shown in Table S1. The PW^{3-} loading of BMImPW(*x*)@MIL-101(Cr) composites were 23.1–50.7 wt%, demonstrating that the "bottle around ship" method is beneficial to make full use of nanocages of MIL-101(Cr) to obtain expected high loading of active PW^{3-}. The BT removal rate of BMImPW(2.0)@MIL-101(Cr) was 92.3%. While for BMImPW(3.5)@MIL-101(Cr), the BT removal rate increased to 95.6%. However, further increase the PW^{3-} loading, the BT removal rate hardly increased, showing the PW^{3-} loading of 39.2% is sufficient. Fig. S1 shows the effect of catalyst dosage on BT ODS removal over BMImPW(*x*)@MIL-101(Cr) with other conditions remained unchanged. BT removal rate was 55.6% at a catalyst dosage (*m*) of 0.01 g. With the increase of *m*, the BT removal rate increased rapidly at first and then slowly, reached a maximum of 95.6% at catalyst dosage of 0.06 g in 90 min. BT removal rate over BMImPW(*x*)@MIL-101(Cr) is 15.1% at 30 °C, showing BT is hardly activated at 30 °C (Fig. S2). With *T* increased 40 °C, the BT removal rate increased to 38.5%, indicating the activation of BT improved greatly. A maximum BT removal rate of 95.6% reached at 50 °C within 90 min. But further increase *T* to 60 °C, BT

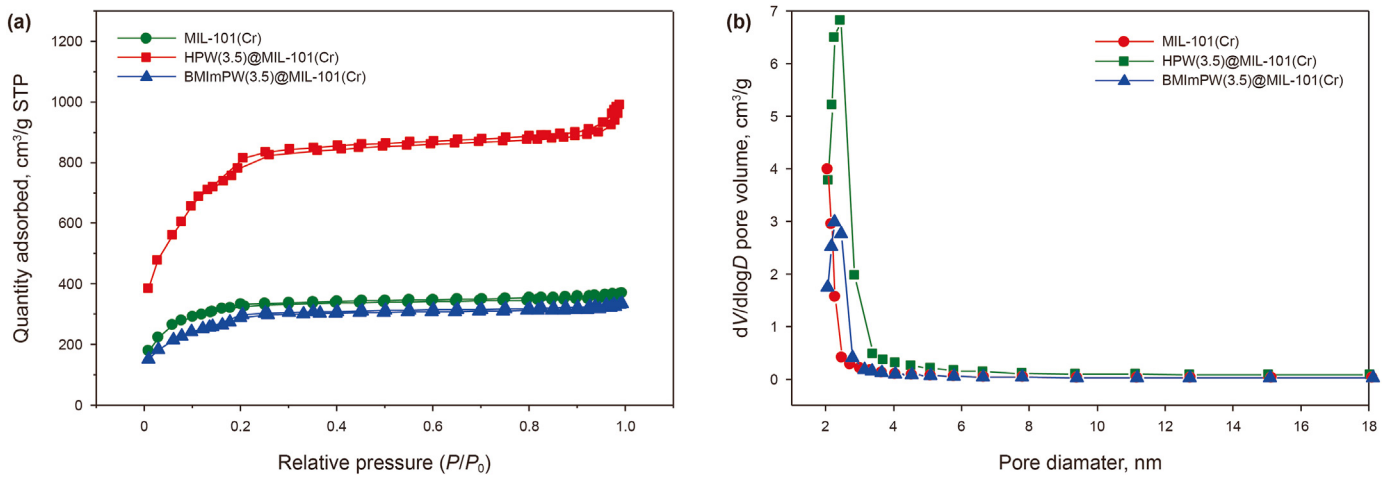

Fig. 4. Typical N_2 adsorption-desorption isotherms (**a**) and pore size distribution (**b**).

Table 2
Structural parameters of samples.

Catalysts	S_{BET}, $m^2 \cdot g^{-1}$	Pore volume, $cm^3 \cdot g^{-1}$	Pore size, nm
MIL-101(Cr)	2465	0.93	3.09
HPW(3.5)@MIL-101(Cr)	1054	0.31	2.67
BMImPW(3.5)@MIL-101(Cr)	928	0.28	2.67

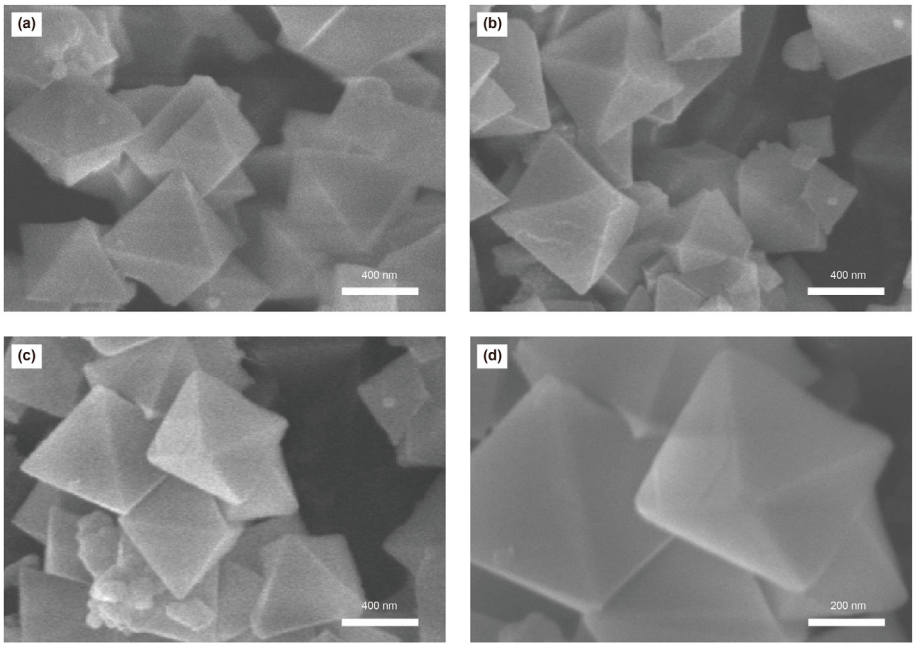

Fig. 5. SEM images of (**a**) MIL-101(Cr), (**b**) HPW(3.5)@MIL-101(Cr), (**c**) BMImPW(3.5)@MIL-101(Cr) and (**d**) BMImPW(3.5)@MIL-101(Cr) (high resolution).

removal decreased slightly. Fig. S3 shows the effect of O/S molar ratio on BT removal rate. The BT removal rate was 38.5% at the O/S molar ratio of 2. With increasing the O/S molar ratio, BT removal rate increased, and reached 95.6% at O/S molar ratio of 8. The BT removal rate was 72.1% in 30 min (Fig. S4). As the reaction time lengthens, BT removal rate increased rapidly and then slowly, reached 100% in 120 min at optimum ODS conditions.

3.2.3. *Effect of different sulfides*

The ODS performances of BMImPW(3.5)@MIL-101(Cr) for various sulfides were studied using 0.012 g/mL of catalyst in model oil and O/S molar ratio of 8 at 50 °C within 60 and 150 min (Fig. 7). The results showed that TP removal onto BMImPW(3.5)@MIL-101(Cr) was low, which was 35.4%, while for the BT, DBT and 4,6-DMDBT were 83.9%, 100% and 96.3%, respectively. The ODS activity of BMImPW(3.5)@MIL-101(Cr) for different sulfides was in the order of DBT > 4,6-DMDBT > BT > TP. The ODS activity is

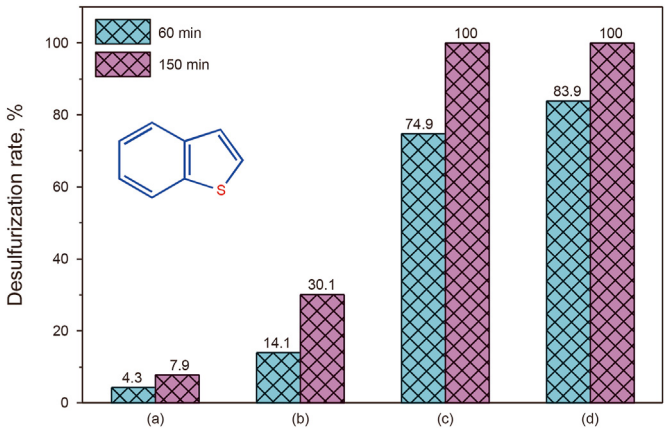

Fig. 6. BT ODS performances of MIL-101(Cr)(**a**), HPW(**b**), HPW(3.5)@MIL-101(Cr)(**c**) and BMImPW(3.5)@MIL-101(Cr)(**d**).
Conditions: 0.012 g/mL of catalyst in model oil, O/S = 8, reacting at 50 °C for 150 min.

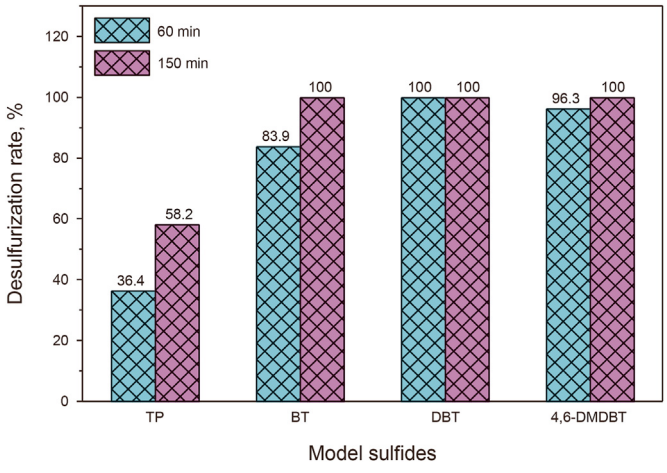

Fig. 7. Comparison of ODS performances of BMImPW(3.5)@MIL-101(Cr) for different model sulfides.
Conditions: 0.012 g/mL of catalyst in model oil, O/S = 8, reacting at 50 °C for 60 and 150 min.

approximately depends on the electron density on the S atom. The electron densities on S atom of TP, BT, DBT and 4,6-DMDBT were 5.696, 5.739, 5.758 and 5.760, respectively. The TP possessed the lowest ODS removal rate among these sulfur compounds owing its lower electron densities on S atom. Te et al. (2001) have studied the relative reactivity of these representative DBTs in oxidation reactions and found that the ODS activity of $Na_3PW_{12}O_{40}$ for representative DBTs was in the order of DBT > 4-MDBT> 4,6-DMDBT owing to the steric hindrance effect. Therefore, the ODS removal of 4,6-DMDBT was slightly lower than that of DBT, which can also be attributed to the steric hindrance effect.

3.3. Recyclability of catalysts

The results of recyclability as prepared BMImPW(3.5)@MIL-101(Cr) were shown in Fig. 8. As can be seen in Fig. 8, the BT removals obtained with fresh BMImPW(3.5)@MIL-101(Cr) and HPW(3.5)@MIL-101(Cr) were both 100.0%. After the seventh cycle, the BT removal of BMImPW@MIL-101(Cr) remained at 96.4%, corresponding to a decrease of only 3.6%. While the BT removal of HPW(3.5)@MIL-101(Cr) dropped to 51.9% after the same number of

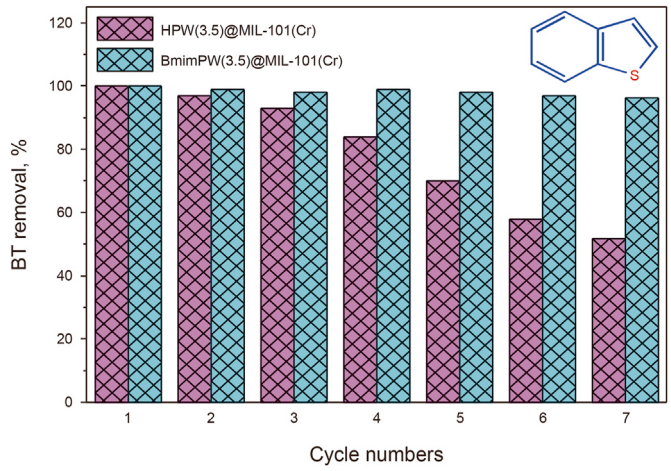

Fig. 8. The recyclability of HPW(3.5)@MIL-101(Cr) and BMImPW(3.5)@MIL-101(Cr).
Conditions: 0.012 g/mL of catalyst in model oil, O/S = 8, reacting at 50 °C on 150 min.

cycles, corresponding to a decrease of 48.1%. Therefore, it can be confirmed that the BMImPW(3.5)@MIL-101(Cr) presented a significantly superior recyclability than HPW(3.5)@MIL-101(Cr), showing that the encapsulation of $BMIm^+$ could effectively increase the stability of the catalyst.

3.4. Theoretical analysis

In order to better explain the unusual stability of BMImPW(3.5)@MIL-101(Cr), the FTIR spectra of fresh, spent and regenerated catalysts (S refer to spent catalyst, R refer to regenerated catalyst and *x* refer to the cycle times) were recorded. As can be seen in Fig. 9(a), for the peaks of MIL-101(Cr) (around 1200–1800 cm^{-1}), no significant changes can be seen for all the HPW(3.5)@MIL-101(Cr)-R*x* (*x* = 3, 5 and 7) as compared to the fresh one. However, with increasing the regeneration time, the intensities of the HPW peaks (around 800–1100 cm^{-1}) for all the HPW(3.5)@MIL-101(Cr)-R*x* are decreased obviously, demonstrating the gradually leaching of HPW after successive cycles of regeneration and reuse. Interestingly, for BMImPW(3.5)@MIL-101(Cr)-R*x* (*x* = 3, 5 and 7), there was no significant change in the intensities of $BMIm^+$ (around 2750–3250 cm^{-1}), MIL-101(Cr) (around 1200–1800 cm^{-1}) and PW^{3-} (around 800–1100 cm^{-1}) (Fig. 9(b)). This revealed that the catalyst structure was well-preserved after successive cycles of regeneration and reuse. More importantly, this also demonstrated the leaching of PW^{3-} was suppressed by addition of $BMIm^+$. This might play an important role in maintaining excellent stability for BMImPW(3.5)@MIL-101(Cr).

The spectra of the HPW(3.5)@MIL-101(Cr)–S7 and BMImPW(3.5)@MIL-101(Cr)–S7 (spent catalyst without regeneration) showed new significant peaks at 1152 and 1288 cm^{-1}, which can be attributed to the sulfone group. This confirmed that the ODS products of BT were the sulfone compounds, which retained inside of the MIL-101(Cr) cavity after ODS. As compared to HPW(3.5)@MIL-101(Cr)–S7 and BMImPW(3.5)@MIL-101(Cr)–S7 without regenerating, the sulfone peak intensities decreased significantly after regeneration. This proved that most of the sulfone could be removed by washing with water.

In order to further explain the unusual stability of the as-prepared BMImPW(3.5)@MIL-101(Cr) catalyst, the XPS analysis are performed with fresh and regenerated samples after successive cycles of regeneration and reuse (Fig. 10 and Table S1). For HPW(3.5)@MIL-101(Cr) (Fig. 10(a)), the O1s peak appeared at 530.08 eV could be attributed to lattice oxygen of Cr–O bonds and

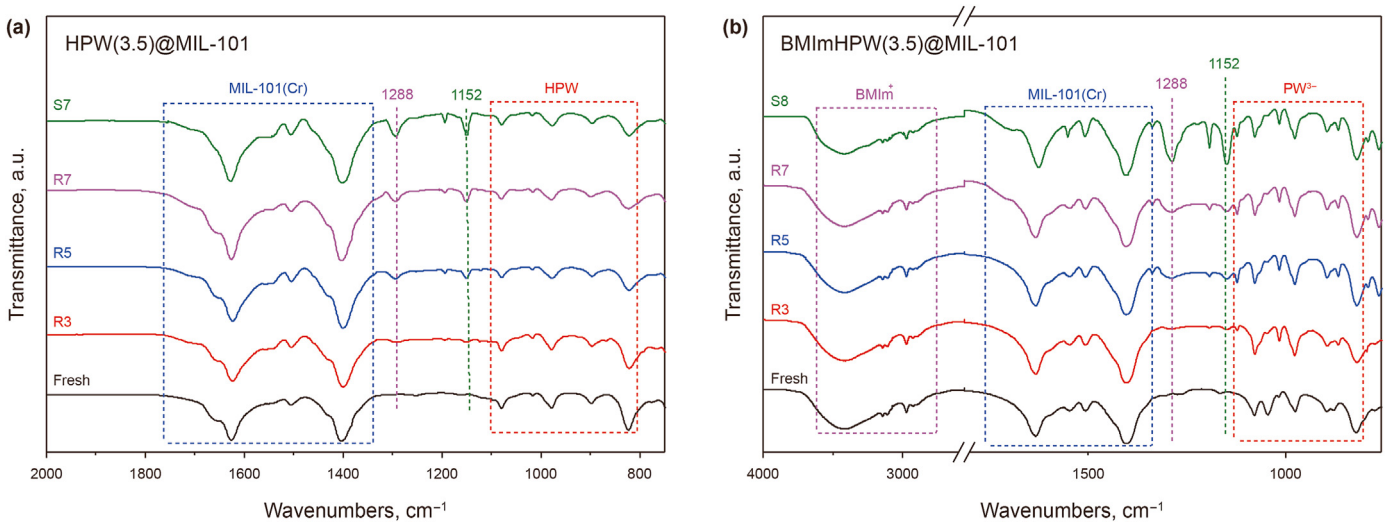

Fig. 9. FTIR spectra of fresh, spent and regenerated HPW(3.5)@MIL-101(Cr) (**a**) and BMImPW(3.5)@MIL-101(Cr) (**b**). (*S* refer to spent catalyst, R refer to regenerated catalyst and *x* refer to the cycle times).

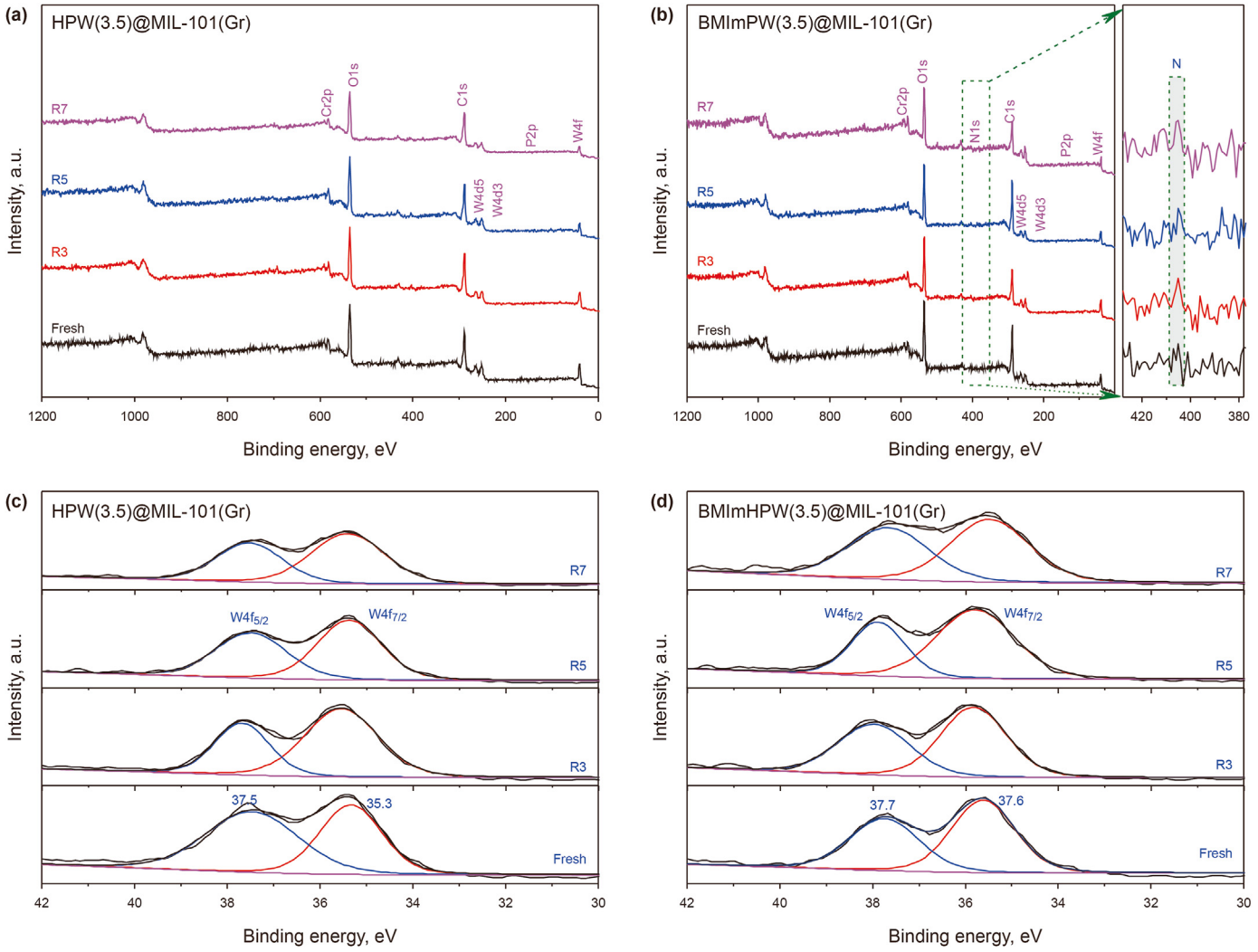

Fig. 10. XPS spectra of HPW(3.5)@MIL-101(Cr) (**a**), BMImPW(3.5)@MIL-101(Cr) (**b**), W4f in HPW(3.5)@MIL-101(Cr) (**c**) and W4f in BMImPW(3.5)@MIL-101(Cr) (**d**) (R refer to regenerated catalyst and *x* refer to the cycle times).

oxygen components of the carboxylate group, while the Cr2p peak appeared at approximately 577.28 eV could be attributed to Cr^{3+} (Zhao et al., 2018). For the BMImPW(3.5)@MIL-101(Cr) (Fig. 10(b)), weak N1s peak appeared at 404.1 eV, which originated from the $BMIm^{+}$. The peaks of O1s and Cr2p were appeared at 530.98 and 578.08 eV, which slightly red shifted as compared to those of the HPW(3.5)@MIL-101(Cr) owing to the introduction of $BMIm^{+}$ (Jin et al., 2009).

As shown in Fig. 10(c), the binding energies of $W4f_{5/2}$ and $W4f_{7/2}$ in HPW(3.5)@MIL-101(Cr) were 35.3 and 37.5 eV, respectively, which could be ascribed to W^{6+} (Wang et al., 2010b). While for the BMImPW(3.5)@MIL-101(Cr) (Fig. 10(d)), the binding energies of $W4f_{5/2}$ and $W4f_{7/2}$ were 35.6 and 37.7 eV, which slightly red shifted as compared to those of the HPW(3.5)@MIL-101(Cr). This might be caused by the effect of $BMIm^{+}$ in the BMImPW(3.5)@MIL-101(Cr). It is worthy to noting that, as compared to fresh HPW(3.5)@MIL-101(Cr), the W^{6+} peak intensities of all the regenerated HPW(3.5)@MIL-101(Cr)-R*x* are decreased obviously with increasing the cycle times, demonstrating the gradually leaching of W species after successive cycles of regeneration and reuse. In contrast, as compared to fresh BMImPW(3.5)@MIL-101(Cr), the total W^{6+} peak intensities of all the regenerated HPW(3.5)@MIL-101(Cr)-R*x* are retained. The well-preserved active PW^{3-} anion ensured the excellent stability of BMImPW(3.5)@MIL-101(Cr) after successive cycles and regeneration.

Elemental contents of fresh and recovered HPW(3.5)@MIL-101(Cr) and BMImPW(3.5)@MIL-101(Cr) catalysts from ICP analysis are listed in Table S2. Similar trends (observed in XPS analysis) were obtained for the both catalysts. Upon introducing of $BMIm^{+}$ to HPW(3.5)@MIL-101(Cr), both $BMIm^{+}$ and PW^{3-} were encapsulated in MIL-101(Cr), forming BMImPW. The PW^{3-} in the BMImPW(3.5)@MIL-101(Cr) was more difficult to leach out as compared to HPW in the HPW(3.5)@MIL-101(Cr) owing the larger size of BMImPW, which evidenced with no obvious leaching in active PW^{3-}. Also, the $BMIm^{+}$ loading was also retained.

To sum up the above analysis, come to the following conclusions: (i) The MIL-101(Cr) structure of catalyst was preserved well after successive cycles of regeneration and reuse. (ii) The valency of active W species of catalysts was not changed after successive cycles of regeneration and reuse. The increased stability of BMImPW(3.5)@MIL-101(Cr) as compared to HPW(3.5)@MIL-101(Cr) may be explained in two ways: (i) The leaching of the active PW^{3-} can be greatly suppressed by forming large size BMImPW (See Fig. 11(a)). (ii) The solubility of BMImPW in water is lower than that of HPW, and therefore, the BMImPW is more difficult to be washed off by water during regeneration as compared to HPW.

According to the structure of 1-methyl-3-butyl-imidazolphotungstate, the possible route of BT ODS over BMImPW(3.5)@MIL-101(Cr) was proposed (Fig. 11): (i) The BT adsorbed firstly onto surface of catalyst. Meanwhile, the BMImPW in catalyst reacts with H_2O_2 in the aqueous phase to form $BMIm^{+}$ cation based peroxytungstate (B) with higher oxidation capacity (Huang et al., 2010a). (ii) BT reacts with the B to form sulfone compound, and the B converted back to BMImPW. (iii) The BMImPW with sulfone compounds is separated by filtration to give clean oil and the solid catalyst was washed with water to remove the sulfone compounds and used for next ODS reaction. The enhanced ODS activity as compared to HPW(3.5)@MIL-101(Cr) may be explained by the intimate contact of BT with active PW^{3-} sites. The $BMIm^{+}$ in catalyst could enhance the lipophilicity of the hydrophilic HPW, which makes the BMImPW(3.5)@MIL-101(Cr) amphiphilic. Besides, both the substituted imidazole cations in BMImPW and the BT possess strong aromatic properties. Due to the strong polarity of the $BMIm^{+}$ cation, which would induce polarization of the discrete π bond in BT. The π-π complexation effect between the polarized π bond with π bond in $BMIm^{+}$ makes the interaction between catalyst and BT enhanced greatly (Zhu et al., 2011). Therefore, the mass transfer of sulfides from oil towards the active HPW sites can greatly accelerate owing to the strong attraction of lipophilic IL to the sulfides (Mirante et al., 2019), increasing the ODS activity by favoring the intimate contact between sulfides in the oil phase and catalyst. Similar results were obtained by Chuang et al. (2012).

4. Conclusion

A novel strategy of combination of “bottle around ship” and “ship in bottle” methods for encapsulation of phosphotungstic acid (HPW) and ionic liquid (BMImBr) inside the mesoporous nanocages of MIL-101(Cr) was proposed for efficient solvent-free ODS. Results indicated that the HPW and BMImBr were successfully encapsulated inside the nanocages of MIL-101(Cr) and the BMImPW@MIL-101(Cr) composites with PW^{3-} loading of 23.1–50.7 wt% were obtained, demonstrating that the “bottle around ship” method is beneficial to make full use of nanocages of MIL-101(Cr) to obtain expected loading of PW^{3-}. The BMImPW(3.5)@MIL-101(Cr)

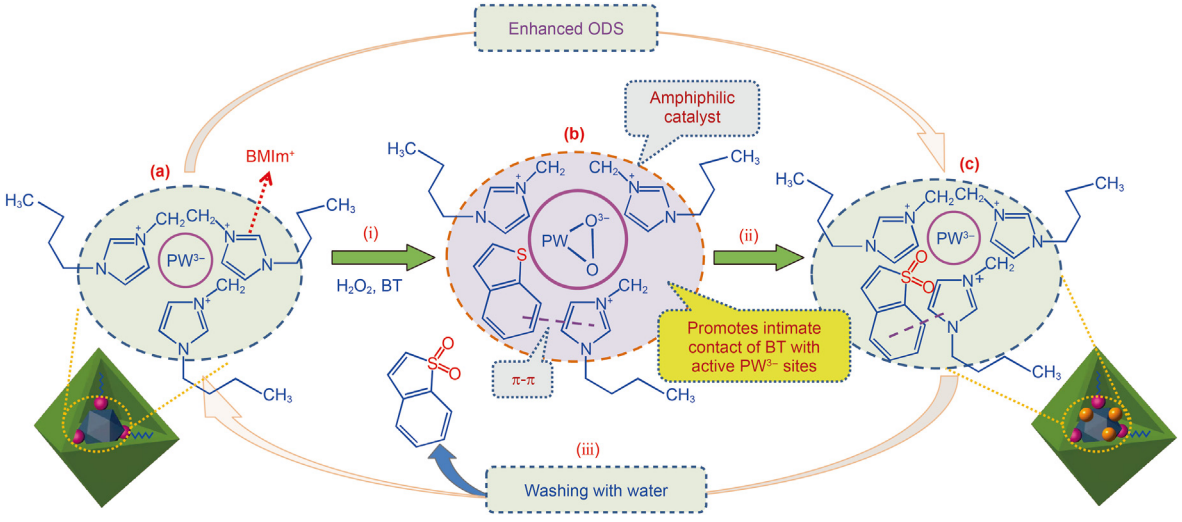

Fig. 11. Possible route of BT ODS over BMImPW(3.5)@MIL-101(Cr)

exhibits excellent reusability with no evidence of leaching of active PW^{3-} and $BMIm^{+}$, and well-preserved structure after successive cycles of regeneration and reuse. The BT removal of BMImPW(3.5)@MIL-101(Cr) remained at 96.0%, corresponding to a 3.6% decrease, while the decrease in BT removal of HPW(3.5)@MIL-101(Cr) was 48.0% after the seventh cycle. The significantly improved stability of BMImPW(3.5)@MIL-101(Cr) as compared to HPW(3.5)@MIL-101(Cr) could be explained by two ways: (i) The introduction of $BMIm^{+}$ ensured the firmly encapsulated active PW^{3-} inside the cavity of MIL-101(Cr) by forming large size BMImPW. Therefore, the leaching of PW^{3-} was suppressed. (ii) The solubility of BMImPW in the water is lower than that of HPW, and thus the loss of active PW^{3-} during regeneration by washing with water decreased by introducing $BMIm^{+}$. The BMImPW(3.5)@MIL-101(Cr) illustrated excellent catalytic activity. A total of 100% BT removal was achieved using 0.06 g of BMImPW(3.5)@MIL-101(Cr) and O/S molar ratio of 8 within 120 min at a reaction temperature of 50 °C. The enhanced ODS activity as compared to HPW(3.5)@MIL-101(Cr) can be explained as follow. The mass transfer of sulfides from oil towards the active HPW sites can greatly accelerate owing to the strong attraction of lipophilic IL to the sulfides, increasing the ODS activity by favoring the intimate contact between sulfides in the oil phase and catalyst.

Appendix A. Supplementary data

Supplementary data to this article can be found online at https://doi.org/10.1016/j.petsci.2023.07.018.

References

Cardoso, L., Gonzaga, A., Aguiar, L., Andrade, H., 2004. Friedel–Crafts acylation of anisole with acetic anhydride over silica-supported heteropolyphosphotungstic acid (HPW/SiO_2). J. Mol. Catal. A. 209, 189–197. https://doi.org/10.1016/j.molcata.2003.08.022.

Chuang, L.L., Huang, J.F., Lo, W.H., Wei, G.T., 2012. Deep desulfurization of light oil through extraction and oxidation processes using H_2O_2/Tungstophosphoric acid in room-temperature ionic liquids. J. Chin. Chem. Soc. 59, 324–330. https://doi.org/10.1002/jccs.201100672.

Ding, J.W., Wang, R., 2016. A new green system of HPW@MOFs catalyzed desulfurization using O_2 as oxidant. Chin. Chem. Lett. 27, 655–658. https://doi.org/10.1016/j.cclet.2016.03.005.

Gu, Y.L., Xu, W., Sun, Y., 2012. Enhancement of catalytic performance over MOF-808(Zr) by acid treatment for oxidative desulfurization of dibenzothiophene. Catal. Today 377, 213–220. https://doi.org/10.1016/j.cattod.2020.10.045.

Hu, X., Lu, Y., Dai, F., Liu, C., Liu, Y., 2013. Host–guest synthesis and encapsulation of phosphotungstic acid in MIL-101 via "bottle around ship": an effective catalyst for oxidative desulfurization. Microporous Mesoporous Mater. 170, 36–44. https://doi.org/10.1016/j.micromeso.2012.11.021.

Huang, W., Zhu, W., Li, H., Shi, H., Zhu, G., Liu, H., Chen, G., 2010. Heteropolyanion-Based ionic liquid for deep desulfurization of fuels in ionic liquids. Ind. Eng. Chem. Res. 49, 8998–9003. https://doi.org/10.1021/ie100234d.

Jin, D., Gao, J., Hou, Z., Guo, Y., Lu, X., Zhu, Y., Zheng, X., 2009. Microwave assisted in situ synthesis of USY-encapsulated heteropoly acid (HPW-USY) catalysts. Appl. Catal. A-Gen. 352, 259–264. https://doi.org/10.1016/j.apcata.2008.10.020.

Juan-Alcaniz, J., Gascon, J., Kapteijn, F., 2012. Metal–organic frameworks as scaffolds for the encapsulation of active species: state of the art and future perspectives. J. Mater. Chem. 22, 10102–10118. https://doi.org/10.1039/c2jm15563j.

Khan, N.A., Bhadra, B.N., Jhung, S.H., 2017. Heteropoly acid-loaded ionic liquid@metal-organic frameworks: effectiveand reusable adsorbents for the desulfurization of a liquid model fuel. Chem. Eng. J. 334, 2215–2221. https://doi.org/10.1016/j.cej.2017.11.159.

Liang, R., Chen, R., Jing, F., Qin, N., Wu, L., 2015. Multifunctional polyoxometalates encapsulated in MIL-100(Fe): highly efficient photocatalysts for selective transformation under visible light. Dalton Trans. 44, 18227–18236. https://doi.org/10.1039/c5dt02986d.

Lee, Y.R., Yu, K., Ravi, S., Ahn, W., 2018. Selective adsorption of rare earth elements over functionalized Cr-MIL-101. ACS Appl. Mater. Interfaces 10, 13918–23927. https://doi.org/10.1021/acsami.8b07130.

Li, A., Lei, J., Du, Y., Guo, Z., Du, X., 2020. Oxidative desulfurization of DBT with H_2O_2 over 3DOM $H_3PW_{12}O_{40}/Al_2O_3$ catalyst. J. Wuhan Univ. Technol. 35, 671–676. https://doi.org/10.1007/s11595-020-2305-6.

Li, A., Song, H., Meng, H., Lu, Y., Li, C., 2019a. Ultrafast desulfurization of diesel oil with ionic liquid based PMoO catalysts and recyclable NaClO oxidant. Chem. Eng. J. 380, 122453. https://doi.org/10.1016/j.cej.2019.122453.

Li, S.W., Gao, R.M., Zhang, R.L., Zhao, J., 2016. Template method for a hybrid catalyst material POM@MOF-199 anchored on MCM-41: highly oxidative desulfurization of DBT under molecular oxygen. Fuel 184, 18–27. https://doi.org/10.1016/j.fuel.2016.06.132.

Li, S.W., Gao, R.M., Zhang, W., Zhang, Y., Zhao, J., 2018. Heteropolyacids supported on macroporous materials POM@MOF-199@LZSM-5. Highly catalytic performance in oxidative desulfurization of fuel oil with oxygen 221, 1–11. https://doi.org/10.1016/j.fuel.2017.12.093.

Li, X., Gu, Y., Chu, H., Ye, G., Zhou, W., Xu, W., Sun, Y., 2019b. MFM-300(V) as an active heterogeneous catalyst for deep desulfurization of fuel oil by aerobic oxidation. Appl. Catal. A-Gen. 584, 117152. https://doi.org/10.1016/j.apcata.2019.117152.

Liu, A., Zhu, M., Dai, B., 2019. A novel high-performance SnO_2 catalyst for oxidative desulfurization under mild conditions. Appl. Catal. A-Gen. 583, 117134. https://doi.org/10.1016/j.apcata.2019.117134.

Liu, Y.W., Liu, S.M., Liu, S.X., Liang, D., Li, S.J., Tang, Q., Wang, X.Q., Miao, J., Shi, Z., Zheng, Z.P., 2013. Facile synthesis of a nanocrystalline metal–organic framework impregnated with a phosphovanadomolybdate and its remarkable catalytic performance in ultradeep oxidative desulfurization. ChemCatChem 5, 3086–3091. https://doi.org/10.1002/cctc.201300378.

Maksimchuk, N.V., Zalomaeva, O.V., Skobelev, I.Y., Kovalenko, K.A., Fedin, V.P., Kholdeeva, O.A., 2012. Metal-organic frameworks of the MIL-101 family as heterogeneous single-site catalysts. Proc. R. Soc. A. 468, 2017–2034. https://doi.org/10.1098/rspa.2012.0072.

Mirante, F., Gomes, N., Branco, L.C., Cunha-Silva, L., Almeida, P.L., Pillinger, M., Gago, S., Granadeiro, G.M., Balula, S., 2018. Mesoporous nanosilica-supported polyoxomolybdate as catalysts for sustainable desulfurization. Microporous Mesoporous Mater. 275, 163–171. https://doi.org/10.1016/j.micromeso.2018.07.036.

Mirante, F., Gomes, N., Corvo, M.C., Gago, S., Balula, S., 2019. Polyoxomolybdate based ionic-liquids as active catalysts for oxidative desulfurization of simulated diesel. Polyhedron 170, 762–770. https://doi.org/10.1016/j.poly.2019.06.019.

Qi, Y., Cai, C., Sun, P., Wang, D., Zhu, H., 2023. Crude oil cracking in deep reservoirs: a review of the controlling factors and estimation methods. Petrol. Sci. 20 (4), 1978–1997. https://doi.org/10.1016/j.petsci.2023.03.006.

Rajati, H., Navarchian, A.H., Tangestaninejad, S., 2018. Preparation and characterization of mixed matrix membranes based on Matrimid/PVDF blend and MIL-101(Cr) as filler for CO_2/CH_4 separation. Chem. Eng. Sci. 185, 92–104. https://doi.org/10.1016/j.ces.2018.04.006.

Rajendran, A., Cui, T.Y., Fan, H.X., Yang, Z.F., Feng, J., Li, W.Y., 2020. A comprehensive review on oxidative desulfurization catalysts targeting clean energy and environment. J. Mater. Chem. A. 8, 2246–2285. https://doi.org/10.1039/C9TA12555H.

Ribeiro, S.O., Granadeiro, C.M., Almeida, P.L., Pires, J., Capel-Sanchez, M.C., Campos-Martin, J.M., Gago, S., Castro, B., Balula, S., 2019. Oxidative desulfurization strategies using Keggin-type polyoxometalate catalysts: biphasic versus solvent-free systems. Catal. Today 333, 226–236. https://doi.org/10.1016/j.cej.2019.122453.

Shan, H.L., Du, Y., Du, X.D., Lei, J.H., 2021. Fabrication of ordered meso-macroporous HPW/TiO_2 catalyst for efficient heterogeneous oxidative desulfurization. J. Wuhan Univ. Technol. 36, 338–346. https://doi.org/10.1007/s11595-021-2414-x.

Shi, D., Xu, L., Chen, P., Ma, T., Lin, C., Wang, X., Xu, D., Sun, J., 2019. Hydroxyl free radical route to the stable siliceous Ti-UTL with extra-large pores for oxidative desulfurization. Chem. Commun. 55, 1390–1393. https://doi.org/10.1039/c8cc09225g.

Te, M., Fairbridge, C., Ring, Z., 2001. Oxidation reactivities of dibenzothiophenes in polyoxometalate-H_2O_2 and formic acid-H_2O_2 systems. Appl. Catal. A-Gen. 219, 267–280. https://doi.org/10.1016/S0926-860X(01)00699-8.

Timko, M.T., Wang, J.A., Burgess, J., Kracke, P., Gonzalez, L., Jaye, C., Fischer, D., 2016. Roles of surface chemistry and structural defects of activated carbons in the oxidative desulfurization of benzothiophenes. Fuel 163, 223–231. https://doi.org/10.1016/j.fuel.2015.09.075.

Wan, H., Chen, C., Wu, Z., Que, Y., Feng, Y., Wang, W., Wang, L., Guan, G., Liu, X., 2015. Encapsulation of heteropolyanion-based ionic liquid within the metal-organic framework MIL-100(Fe) for biodiesel production. ChemCatChem 7, 441–449. https://doi.org/10.1002/cctc.201402800.

Wang, D., Lu, S., Jiang, S.P., 2010b. Pd/HPW-PDDA-MWCNTs as effective non-Pt electrocatalysts for oxygen reduction reaction of fuel cells. Chem. Commun. 46, 2058–2060. https://doi.org/10.1039/b927375a.

Wang, H.W., Jibrin, I., Zeng, X.Y., 2020. Catalytic oxidative desulfurization of gasoline using phosphotungstic acid supported on MWW zeolite. Front. Chem. Sci. Eng. 14, 546–560. https://doi.org/10.1007/s11705-019-1842-z.

Wang, J., Zhao, D., Li, K., 2010a. Oxidative desulfurization of dibenzothiophene using ozone and hydrogen peroxide in ionic liquid. Energy Fuel. 24, 2527–2529. https://doi.org/10.1021/ef901324p.

Wang, X.S., Huang, Y.B., Lin, Z.J., Cao, R., 2014. Phosphotungstic acid encapsulated in the mesocages of amine-functionalized metal-organic frameworks for catalytic oxidative desulfurization. Dalton Trans. 43, 11950–11958. https://doi.org/10.1039/c4dt01043d.

Xu, S., Wang, M., Feng, B., Han, X., Lan, Z., Gu, H., Li, H., Li, H., 2018. Dynamic kinetic resolution of amines by using palladium nanoparticles confined inside the cages of amine-modified MIL-101 and lipase. J. Catal. 363, 9–17. https://doi.org/10.1016/j.jcat.2018.04.006.

Yuan, D., Song, H., Song, H., You, M., Wang, B., Li, F., Hao, Y., Yu, Q., 2017.

Heterogeneous oxidative desulfurization for model fuels using novel PW-coupled polyionic liquids with carbon chains of different lengths. J. Taiwan Inst. Chem. Eng. 76, 83–88. https://doi.org/10.1016/j.jtice.2017.04.013.

Yue, D., Lei, J., Lina, Z., Guo, Z., Du, X., Li, J., 2018. Oxidation desulfurization of fuels by using amphiphilic hierarchically meso/macroporous phosphotungstic acid/SiO_2 catalysts. Catal. Lett. 148, 1100–1109. https://doi.org/10.1007/s10562-018-2317-4.

Zhang, D.X., Song, H., Yuan, D.D., 2019b. Synthesis of highly dispersed phosphotungstic acid encapsulated in MIL-100(Fe) catalyst and its performance in heterogeneous oxidative desulfurization. Chem. Eng. Commun. 206, 1706–1714. https://doi.org/10.1080/00986445.2019.1573167.

Zhang, F., Jin, Y., Shi, J., Zhong, Y., Zhu, W., El-Shall, M.S., 2015. Polyoxometalates confined in the mesoporous cages of metal–organic framework MIL-100(Fe): efficient heterogeneous catalysts for esterification and acetalization reactions. Chem. Eng. J. 269, 236–244. https://doi.org/10.1016/j.cej.2015.01.092.

Zhang, M., Liu, J.Q., Li, H.P., Wei, Y., Fu, Y., Liao, W., Zhu, L., Chen, G., Zhu, W., Li, H., 2020. Tuning the electrophilicity of vanadium-substituted polyoxometalate based ionic liquids for high-efficiency aerobic oxidative desulfurization. Appl. Catal. B Environ. 271, 118936. https://doi.org/10.1016/j.apcatb.2020.118936.

Zhang, Q., Zhang, J., Yang, H., Dong, Y., Liu, Y., Yang, L., Wei, D., Wang, W., Bai, L., Chen, H., 2019a. Efficient aerobic oxidative desulfurization over Co-Mo-O bimetallic oxide catalysts. Catal. Sci. Technol. 9, 2915–2922. https://doi.org/10.1039/c9cy00459a.

Zhao, S., Mei, J., Xu, H., Liu, W., Qu, Z., Cui, Y., Yan, N., 2018. Research of mercury removal from sintering flue gas of iron and steel by the open metal site of Mil-101(Cr). J. Hazard Mater. 351, 301–307. https://doi.org/10.1016/j.jhazmat.2017.12.016.

Zhu, C., Jiang, F., Zhang, P., Zhao, Z., Chen, X., Wu, Y., Chen, Y., Wang, W., Song, Z., Hu, T., Xu, T., Zhou, Y., 2023. Effect of petroleum chemical fraction and residual oil content in saline lacustrine organic-rich shale: a case study from the Paleogene Dongpu Depression of North China. Petrol. Sci. 20, 649–669. https://doi.org/10.1016/j.petsci.2022.09.013.

Zhu, M., Luo, G., Kang, L., Dai, B., 2014. Novel catalyst by immobilizing a phosphotungstic acid on polymer brushes and its application in oxidative desulfurization. RSC Adv. 4, 16769–16776. https://doi.org/10.1039/c4ra01367k.

Zhu, W., Huang, W., Li, H., Zhang, M., Jiang, W., Chen, G., Han, C., 2011. Polyoxometalate-based ionic liquids as catalysts for deep desulfurization of fuels. Fuel Process. Technol. 92, 1842–1848. https://doi.org/10.1016/j.fuproc.2011.04.030.

Zhu, Y., Zhu, M., Kang, L., Yu, F., Dai, B., 2015. Phosphotungstic acid supported on mesoporous graphitic carbon nitride as catalyst for oxidative desulfurization of fuel. Ind. Eng. Chem. Res. 54, 2040–2047. https://doi.org/10.1021/ie504372p.